HHS Public Access

Author manuscript

Cancer Res. Author manuscript; available in PMC 2020 April 15.

Published in final edited form as:

Cancer Res. 2019 April 15; 79(8): 1967–1980. doi:10.1158/0008-5472.CAN-18-1787.

MYC drives Group 3 medulloblastoma through transformation of Sox2+ astrocyte progenitor cells

Ran Tao[1], **Najiba Murad**[1], **Zhenhua Xu**[1], **Peng Zhang**[2], **Konstantin Okonechnikov**[3,4], **Marcel Kool**[3,4], **Samuel Rivero-Hinojosa**[1], **Christopher Lazarski**[1], **Pan Zheng**[2], **Yang Liu**[2], **Charles G. Eberhart**[5], **Brian R. Rood**[1], **Roger Packer**[1], and **Yanxin Pei**[1,*]

[1]Center for Cancer and Immunology, Brain Tumor Institute, Children's National Health System, USA

[2]Division of Immunotherapy, Institute of Human Virology, School of Medicine, University of Maryland, USA

[3]Hopp Children's Cancer Center at the NCT Heidelberg (KiTZ)

[4]Division of Pediatric Neuro-oncology of the German Cancer Research Center (DKFZ) and German Cancer Consortium (DKTK), Germany

[5]Division of Neuropathology, Johns Hopkins University, USA.

Abstract

A subset of Group 3 medulloblastoma frequently harbors amplification or overexpression of *MYC* lacking additional focal aberrations, yet it remains unclear whether *MYC* overexpression alone can induce tumorigenesis and which cells give rise to these tumors. Here, we showed that astrocyte progenitors in the early postnatal cerebellum were susceptible to transformation by *MYC*. The resulting tumors specifically resembled human Group 3 medulloblastoma based on histology and gene expression profiling. Gene expression analysis of *MYC*-driven medulloblastoma cells revealed altered glucose metabolic pathways with marked overexpression of lactate dehydrogenase A (*LDHA*). *LDHA* abundance correlated positively with *MYC* expression and was associated with poor prognosis in human Group 3 medulloblastoma. Inhibition of LDHA significantly reduced growth of both mouse and human *MYC*-driven tumors but had little effect on normal cerebellar cells or SHH-associated medulloblastoma. By generating a new mouse model, we demonstrated for the first time that astrocyte progenitors can be transformed by *MYC* and serve as the cells of origin for Group 3 medulloblastoma. Moreover, we identified *LDHA* as a novel, specific therapeutic target for this devastating disease.

Keywords

medulloblastoma; cell-of-origin; mouse model; MYC; LDHA

[*]**Correspondence:** Yanxin Pei, Address: Children's National Health System, 111 Michigan Ave NW, Washington, DC 20010, ypei@childrensnational.org, Telephone: 202-476-2558, Fax: 202-476-6994.

Disclosures: The authors declare no existing or potential conflicts of interest.

Introduction

Medulloblastoma is a highly malignant tumor of the cerebellum that occurs most frequently in children [1]. Medulloblastoma is widely recognized as comprising four molecular subgroups termed WNT, SHH, Group 3 and Group 4 [2–4]. Recently, Group 3 medulloblastoma has been further divided into three subtypes, distinguished by distinct gene copy number aberrations, somatic mutations, potential oncogenic drivers and clinical outcomes [5]. Group 3α tumors frequently involve loss of *MYC*, group 3β tumors exhibit activation of *GFI1* and *GFI1B,* and group 3γ tumors harbor *MYC* amplification or overexpression in the absence of other focal aberrations [6]. Another recent study identified four subtypes of tumors in Group 3 medulloblastoma, in which subtype II is associated with *MYC* amplification [2]. Despite aggressive treatment, over 70% of patients with *MYC*-amplified medulloblastoma succumb to the disease [5]. Moreover, surviving patients often suffer severe treatment-related side effects, including permanent cognitive and motor disabilities. Thus, there is a critical need for novel targeted therapies that not only improve life expectancy, but also limit damage to healthy brain tissue. The development of such therapies necessitates an animal model that accurately recapitulates the molecular and cellular hallmarks of Group 3 medulloblastoma subtypes.

In recent years several animal models have been generated. For example, one model generated from $CD133^+$ cells overexpressing *Myc* and *Gfi1* [7] may represent group 3β tumors. Other models involve *Myc* overexpression in combination with *Trp53* inactivation in either $CD133^+$ cells or $Math1^+$ granule neuron progenitors (GNPs) [7–10]. However, mutation or deletion of *TP53* is rarely detected in human Group 3 medulloblastoma at diagnosis [11, 12], indicating that loss of function of *TP53* is not required for human tumor initiation. Mouse models featuring *Trp53* mutation may thus be of limited relevance for understanding human tumor biology and therapy development.

Since group 3γ tumors frequently harbor *MYC* amplification without additional focal mutations, it is of interest to determine whether *MYC* overexpression alone can initiate tumor formation in the developing cerebellum. *MYC* alone was thought incapable of inducing neoplastic transformation because high levels of *MYC* drive apoptosis [13, 14]. However, it is now clear that *MYC*-induced apoptosis and tumor initiation depend upon cell type and developmental context [15–17]. Medulloblastomas are thought to originate from immature cells at an early stage of cerebellar development, and different subgroups of medulloblastoma have distinct cell origins. WNT subgroup tumors originate from progenitor cells in the lower rhombic lip of the brainstem [18] while SHH tumors arise from GNPs in the external granular layer (EGL) [19, 20]. In contrast, the cell-of-origin for Group 3 medulloblastoma has not yet been well characterized. Here, we showed that *MYC* overexpression was sufficient to drive tumorigenesis in astrocyte progenitors in the early postnatal cerebellum in mice. The resulting tumors accurately resembled human Group 3 medulloblastoma in terms of histology and gene expression, suggesting that astrocyte progenitors in the early postnatal cerebellum may represent the cell-of-origin for Group 3 medulloblastoma.

In the course of analyzing our new mouse model of *MYC*-driven medulloblastoma, we discovered that key genes involved in glycolysis were significantly upregulated in *MYC*-driven tumors compared to normal cerebellar tissue or SHH-associated medulloblastoma. Of these genes, *LDHA* (encoding lactate dehydrogenase A) expression was positively correlated with *MYC* and was associated with poor prognosis in Group 3 medulloblastoma. Furthermore, inhibition of *LDHA* significantly suppressed growth of *MYC*-driven medulloblastoma, but had little effect on the growth of SHH-associated medulloblastoma or viability of normal cerebellar cells. Thus, our studies identify *LDHA* as a novel, specific target for *MYC*-driven medulloblastoma treatment.

Materials and Methods

Animals

Aldh1L1^{-GFP} mice were provided by Dr. Jeffery Rothstein (John's Hopkins University School of Medicine); Aldh1L1-CreER^{T2} mice were provided by Dr. Baljit Khakh (University of California, Los Angeles); Math1^{-GFP}, Sox2^{-GFP}, Sox2-CreER^{T2}, Sox2^{-loxp}, Rosa-CAG-LSL-tdTomato, **N**OD-**S**CID-IL2R**G**amma null (NSG) and C57BL/6J mice were purchased from the Jackson Laboratory. Mice were maintained in the Animal Facility at Children's National Health System (CNHS). All experiments were performed in accordance with national guidelines and regulations, and with the approval of the animal care and use committee at CNHS.

Tumor Generation

To generate tumors, we isolated total cerebellar cells from P5 mice of C57BL/6J, Sox2-CreER^{T2}/Rosa-CAG-LSL-tdTomato, Sox2-CreER^{T2} or Sox2-CreER^{T2}/Sox2^{-loxp}; or we FACS-sorted cells from P5 mice of C57BL/6J, Sox2^{-GFP}, or Sox2-CreER^{T2}/Aldh1L1^{-GFP}/Rosa-CAG-LSL-tdTomato. These cells were infected with the indicated viruses and cultured overnight in NeuroCult™ medium (Stemcell Technologies) supplemented with Proliferation Supplement (Stemcell Technologies), basic fibroblast growth factor (bFGF) and epidermal growth factor (EGF) (Peprotech). Cells were then injected into the cerebella of NSG mice (6–8 weeks old) using a stereotaxic frame with a mouse adaptor (David Kopf Instruments), as described previously [8]. To permanently label Sox2^{+} cells with tdTomato, total cerebellar cells from P5 Sox2-CreER^{T2}/ Rosa-CAG-LSL-tdTomato mice were cultured with 100 nM 4-hydroxytamoxifen (Sigma) overnight. To knockout *Sox2* in Sox2^{+} cerebellar cells, total cerebellar cells from P5 Sox2-CreER^{T2}/Sox2^{-loxp} mice were cultured with 100 nM 4-hydroxytamoxifen overnight. After transplantation, animals were treated with tamoxifen for an additional 6 days to ensure complete *Sox2* deletion. Mice receiving mock treated Sox2-CreER^{T2}/Sox2^{-loxp} cells or 4-hydroxytamoxifen treated Sox2-CreER^{T2} cells were used as controls. The mice receiving 4-hydroxytamoxifen treated Sox2-CreER^{T2} cells were also treated with tamoxifen for additional 6 days post-transplantation.

Glycolysis Pathway Inhibition Assays

To assess the effects of small molecule inhibitors of glucose metabolism on cell growth, tumor cells were freshly isolated from tumor-bearing mice and treated with the indicated concentrations of GSK 2837808a (Tocris Bioscience), FX11 (Calbiochem), PKI-III

(Calbiochem) or DCA (Tocris Bioscience). Cells were cultured in 384-well Greiner plates for 7 days in stem cell medium (Neurobasal Media-Vitamin A + DMEM/F12 + Non Essential Amino Acids + Sodium pyruvate + Hepes + GlutaMAX + Pen-Strep + B27 + EGF + bFGF + Lif + Heparin). Cell viability was then assessed using CellTiter-Glo® assay (Promega). To determine the effects of GSK 2837808a on cell viability of normal cells, mouse GNPs were cultured for 7 days on poly D-lysine-coated plates with NeuroBasal™ medium (Life Technologies) supplemented with B27 (Gibco), SHH (Peprotech) and 2% FBS and containing the indicated concentration of GSK 2837808a. Cell viability was then assessed using CellTiter-Glo® assay.

LDHA Knockdown

To assess the effects of *LDHA* knockdown on cell growth of human Group 3 or SHH Group medulloblastoma *in vitro*, freshly isolated patient-derived xenograft (PDX) tumor cells were infected with retrovirus encoding *LDHA* shRNA or corresponding control shRNA overnight. Cells were then cultured in stem cell medium for an additional 2 or 6 days. Cell viability was assessed using the CellTiter-Glo® assay.

To test the effects of *LDHA* knockdown on growth of human Group 3 medulloblastoma *in vivo*, freshly isolated tumor cells were infected with retrovirus encoding *LDHA* shRNA or corresponding control shRNA overnight. Cells were then injected into the cerebella of NSG mice (50,000 cells per mouse). Mice were sacrificed once they exhibited symptoms. Animal survival was assessed by Kaplan-Meier curve.

Mouse Cells and Patient-Derived Xenografts

All mouse tumor cells or normal cells were freshly isolated from the indicated mice. PDX lines used for this study include: MB002 (G3) generated by the Cho lab [21]; ICb-984 (SHH) generated by the Li lab [22]; Med-411-FH (G3) and Med-211-FH (G3) generated by the Olson lab [23, 24]; RCMB20 (G3), RCMB40 (G3) and RCMB28 (G3) generated by the Wechsler-Reya lab [25]. PDX lines were generated by implanting patient cells directly into the cerebella of immune-compromised mice, and propagating them from mouse to mouse without *in vitro* passaging. The identity and subgroup of each line was validated by gene expression and/or methylation analysis. We did not perform testing for mycoplasma.

Accession Numbers

RNA-Seq data have been deposited in the GEO public database (http://www.ncbi.nlm.nih.gov/geo/), with accession number GSE114760.

Results

Overexpression of *MYC* Alone is Sufficient to Initiate Tumorigenesis in the Cerebellum

To investigate whether overexpression of the *MYC* oncogene alone is sufficient to initiate tumorigenesis, we isolated total cerebellar cells from C57BL/6J mice at postnatal day 2–7 (P2–7), as opposed to isolating specific cell populations as was done previously [8, 9]. In addition, we infected the cells with *MYC* lentivirus rather than retrovirus, allowing both quiescent and proliferating cells to be transduced. We cultured *MYC*-infected cerebellar

cells for 16 hours and then transplanted the cells into the cerebella of NSG mice. Tumor growth was monitored *in vivo* using bioluminescence imaging to detect the expression of luciferase protein encoded by the lentivirus vector. Most animals exhibited strong luciferase signal in the cerebellum and developed tumors within 60 days post transplantation (Fig. 1A and 1B). Staining of tumor tissue with hematoxylin and eosin (H&E) showed large cell/anaplastic (LCA) histology, with nuclear molding and wrapping, focally prominent nucleoli, abundant mitotic and apoptotic cells as well as necrotic foci (Fig. 1C and Supplementary Fig.S1A), typical features of Group 3 medulloblastoma. Immunohistochemistry (IHC) staining showed that these tumors were highly proliferative ($Ki67^+$) and apoptotic (cleaved caspase-3, $CC\text{-}3^+$). Some tumor cells expressed neuronal marker Synaptophysin and rare tumor cells expressed glial marker glial fibrillary acidic protein (GFAP) (Supplementary Fig. S1B–E). These findings suggest that *MYC* overexpression alone is sufficient to induce Group 3-like medulloblastoma in the postnatal cerebellum, but the identity of the cell population(s) susceptible to *MYC*-driven transformation had yet to be defined.

$Sox2^+$ Cells in the Postnatal Cerebellum are Susceptible to Transformation by *MYC*

$Sox2^+$ cells represent stem cell/progenitors in the early postnatal cerebellum, but their ability to form *MYC*-driven medulloblastoma has never been evaluated. We thus examined whether these cells could be transformed by *MYC*. We first evaluated Sox2 expression in cerebella of P5 C57BL/6J and $Sox2^{-GFP}$ mice [26] and found abundant $Sox2^+$ cells located in the Purkinje Cell Layer (PCL), White Matter Folium (WMF) and Deep White Matter (DWM) but not in the EGL (Supplementary Fig. S1F–H). We then examined proliferation and apoptosis of $Sox2^+$ cells after transduction with *MYC*. FACS-sorted GFP^+ cells from the cerebella of P5 $Sox2^{-GFP}$ mice (Fig. 1D) were infected with lentivirus encoding doxycycline (Dox) inducible *MYC*. *MYC* overexpression (Dox+) resulted in a significant increase in proliferation, but little change in apoptosis compared to cells without *MYC* overexpression (Dox-) (Supplementary Fig. S1I and J). When the *MYC*-transduced $Sox2^+$ cells were transplanted into the cerebella of NSG mice, they developed highly aggressive tumors. In contrast, *MYC*-transduced $Sox2^-$ cells rarely developed tumors (Fig. 1E), suggesting that $Sox2^+$ cells in the postnatal cerebellum are susceptible to *MYC* induced transformation.

Most $Sox2^+$ cells were observed to be quiescent, but a small population of $Sox2^+$ cells was observed to be proliferative in the postnatal cerebellum (Supplementary Fig. S1K). Lentivirus can infect both quiescent and proliferating cells, but retrovirus only infects proliferating cells. To evaluate whether *MYC*-driven tumors arise from quiescent or proliferative $Sox2^+$ cells, we transplanted $Sox2^+$ cells infected with *MYC* retrovirus into the cerebella of NSG mice. Our results showed that almost all mice receiving $Sox2^+$ cells infected with *MYC* lentivirus developed tumors, but $Sox2^+$ cells infected with *MYC* retrovirus did not give rise to tumors (Supplementary Fig. S1L), indicating that the quiescent $Sox2^+$ cells are the target of *MYC*-induced tumorigenesis in this study.

We then validated $Sox2^+$ cells as the major cell population susceptible to *MYC*-induced transformation by an alternative approach. Sox2-$CreER^{T2}$ mice [26] were crossed with Rosa-CAG-LSL-tdTomato mice [27] and total cerebellar cells were isolated from P5 progeny. Cells were infected with *MYC* lentivirus and treated with 4-hydroxytamoxifen (4-

OHT) to activate CreER^{T2} and permanently label Sox2$^+$ cells with tdTomato (tdT). Cells were then transplanted into the cerebella of NSG mice. Under these conditions, we hypothesized that tumors arising specifically from Sox2$^+$ cells will exhibit universal tdT expression. If tumors arise from both Sox2$^+$ and Sox2$^-$ cells, only a fraction of cells within a given tumor will express tdT; or if tumors develop from Sox2$^-$ cells, the tumor will be tdT$^-$ (Fig. 1F). We first examined whether tdT expression specifically labeled Sox2$^+$ cells and their progeny after tamoxifen treatment. We treated mice with tamoxifen at P5 and found that tdT expression was specifically observed in Sox2$^+$ cells at P6 (Supplementary Fig. S2A) and tdT expression remained stable even after *Sox2* expression ceased during cerebellar development at P10 (Supplementary Fig. S2B). Further studies revealed that mice receiving cells without 4-OHT treatment all developed tdT$^-$ tumors and all animals receiving cells treated with 4-OHT developed tumors with nearly universal tdT expression (Fig. 1G and H), indicating that *MYC*-driven tumors originate specifically from Sox2$^+$ cells in this system. tdT$^+$ and tdT$^-$ tumors were otherwise indistinguishable on the basis of IHC staining for markers as described above (Supplementary Fig. S2C).

Tumors Generated from Sox2$^+$ cells Resemble Human Group 3 Medulloblastoma

We characterized the tumors arising from Sox2$^+$ cells (hereafter referred to as SOX2 tumors) at the cellular and molecular levels. SOX2 tumors exhibited LCA histology, high proliferation index, abundant apoptosis and strong MYC expression (Fig. 2A–D), suggesting they may represent Group 3 medulloblastoma. A small number of tumor cells were positive for Synaptophysin or GFAP (Fig. 2E and F). Few tumor cells expressed Sox2 and a large number of cells were Olig2$^+$ (Fig. 2G and H). Olig2 expression was also observed in a subset of human Group 3 medulloblastoma PDX (Fig. 2I–L).

To determine whether these tumors resemble Group 3 medulloblastoma at the molecular level, we performed RNA-Seq analysis on mouse *MYC*-driven tumors and compared the gene expression profiles with those of 167 human tumor samples from a recent global medulloblastoma study [2]. The comparative analysis was based on strict selection of 17039 orthologous genes and precise batch effect adjustment to address species differences. Principal component analysis (PCA) and/or hierarchical clustering showed that mouse *MYC*-driven tumors generated from total cerebellar cells (TC tumor) or Sox2$^+$ cells (SOX2 tumor) were similar and indistinguishable from human Group 3 medulloblastoma at the level of gene expression (Fig. 2M and N, Supplementary Fig S3A, and Supplementary Table S1–3). They also demonstrated strong similarity to previous models of *Myc* + *DNp53* tumor (MP tumor) and *Myc* + *Gfi1*/*Gfi1b* tumor (MG/MGb tumor) (Supplementary Fig. S3B and Supplementary Table S4). Specifically, mouse SOX2 tumors statistically resembled human *MYC*-amplified Group 3 medulloblastoma (Fig. 2M and Supplementary Fig. S3C). Further analysis revealed correspondence of SOX2 tumors mainly to Group 3 subtype II medulloblastoma associated with *MYC* amplification [2] (Fig. 2O).

We also analyzed marker genes characterizing medulloblastoma molecular subgroups including *DKK1* (WNT Group), *SFRP1* (SHH Group), *NPR3* (Group 3) and *KCNA1*, *CDK6, MYCN* (Group 4). *DKK1* was not detected in SOX2 tumors. *SFRP1* was significantly decreased in SOX2 tumors compared to normal cerebellar cells, suggesting that

these are non-SHH subgroup tumors. Very low or almost no detectable expression of *KCNA1, CDK6* and *MYCN* in SOX2 tumors suggests that these tumors do not model Group 4 medulloblastoma. In contrast, *NPR3* was significantly upregulated in SOX2 tumors compared to normal cerebellar cells (Supplementary Table S5). In addition, no *Trp53* mutation or *Gfi1* overexpression was observed in SOX2 tumors (Supplementary Fig. S3D and E).

MYC-driven Tumors Arise from Astrocyte Progenitors

The observation of Sox2 expression in distinct areas of the cerebellum prompted the question of whether Sox2 is expressed in distinct cell lineages, one or more of which is able to give rise to *MYC*-driven tumors. We found that Aldh1L1, which is a glial marker, can be used to distinguish different population of $Sox2^+$ cells. In the cerebellum of P5 $Aldh1L1^{-GFP}$ mice [28], $Sox2^+$ cells in the PCL expressed strong GFP (Fig. 3A and B) while most $Sox2^+$ cells in the DWM expressed weak GFP and a fraction of $Sox2^+$ cells in this area were GFP^- (Fig. 3C and D). Further analysis showed that the $Sox2^+$/ $Aldh1L1^{neg}$ cells in the DWM expressed Olig2 (Fig. 3E–H). Using $Aldh1L1^{-GFP}$/Sox2-$CreER^{T2}$/Rosa-CAG-LSL-tdTomato mice, we could divide $Sox2^+$ cells into three populations: tdT^+/GFP^{high} ($Sox2^+/Aldh1L1^{high}$), tdT^+/GFP^{low} ($Sox2^+/Aldh1L1^{low}$) and tdT^+/GFP^{neg} ($Sox2^+/Aldh1L1^{neg}$) cells (Fig. 3I).

To characterize $Sox2^+/Aldh1L1^{high}$, $Sox2^+/Aldh1L1^{low}$ and $Sox2^+/Aldh1L1^{neg}$ cells, we FACS-sorted these cells (Fig. 3I and Supplementary Fig. S4A) and evaluated their self-renewal and differentiation potential *in vitro*. $Sox2^+/Aldh1L1^{high}$ cells exhibited the highest frequency of neurosphere formation, while very few neurospheres arose from $Sox2^+/Aldh1L1^{low}$ and almost no neurospheres were observed from $Sox2^+/Aldh1L1^{neg}$ cells (Fig. 3J and Supplementary Fig. S4B). $Sox2^+/Aldh1L1^{high}$ cells formed secondary spheres but could not generate tertiary spheres (Fig. 3K). Instead, they formed an adherent cell layer with astrocytic morphology (Supplementary Fig. S4C), indicating they were incapable of long-term self-renewal. When primary neurospheres were cultured in differentiation medium, they differentiated exclusively into astrocytes ($GFAP^+$). No neurons ($NeuN^+$), interneurons ($Pax2^+$) or oligodendrocytes ($O4^+$) were observed (Fig. 3L). Furthermore, freshly isolated $Sox2^+/Aldh1L1^{high}$, $Sox2^+/Aldh1L1^{low}$, and $Sox2^+/Aldh1L1^{neg}$ cells cultured in differentiation medium gave rise predominantly to astrocytes, interneurons and oligodendrocytes respectively (Supplementary Fig. S4D and E). These results suggest that $Sox2^+$ cells are composed of three distinct lineages and $Sox2^+/Aldh1L1^{high}$ cells are unipotent astrocyte progenitors capable of short-term self-renewal. *In vivo* lineage tracing studies revealed that $Aldh1L1^+$ cells differentiated into astrocytes and interneurons in the early postnatal cerebellum (Supplementary Fig. S4F and G), consistent with our *in vitro* observations. We then examined the potential of each cell population to generate tumors and found that tumors primarily arose from $Sox2^+/Aldh1L1^{high}$ cells. Rare tumors arose from $Sox2^+/Aldh1L1^{low}$ cells, with lower penetrance and longer latency. $Sox2^+/Aldh1L1^{neg}$ cells did not develop tumors (Fig. 3M). These findings strongly suggest that *MYC*-driven tumors originate from astrocyte progenitors.

A previous study showed that $CD133^+$ cells in the postnatal cerebellum consist of glial progenitors [29]. We thus examined whether Sox2 and CD133 were expressed in the same cells. Among total cerebellar cells, approximately 4% were $CD133^+$ and 20% were $Sox2^+$. However, only 10% of $Sox2^+$ cells were $CD133^+$, indicating that while CD133 and Sox2 markers indeed overlap to some degree, Sox2 expression identifies a distinct population(s) of cells (Fig. 4A and B). We then characterized $Sox2^+/CD133^+$, $Sox2^+/CD133^-$ and $Sox2^-/CD133^+$ populations by evaluating self-renewal, differentiation, expression of lineage markers and potential for tumorigenesis. Neurospheres were generated from $Sox2^+/CD133^+$ cells and $Sox2^+/CD133^-$ cells, but not from $Sox2^-/CD133^+$ cells (Fig. 4C). When neurospheres were cultured in differentiation medium, they differentiated exclusively into astrocytes, suggesting that the cells capable of self-renewal are astrocyte progenitors (Fig. 4D). Flow cytometry analysis showed that neuron progenitors (PSA-$NCAM^+$) and oligodendrocyte progenitors ($O4^+$) [29] were enriched in $Sox2^-/CD133^+$ cells, but not in $Sox2^+/CD133^+$ or $Sox2^+/CD133^-$ cells (Supplementary Fig. S5A). $Sox2^+/CD133^+$ and $Sox2^+/CD133^-$ cells infected with *MYC* lentivirus developed tumors, while $Sox2^-/CD133^+$ cells did not (Fig. 4E). Although a subpopulation of $CD133^+$ cells express Sox2, but $CD133^+$ cells infected with *Myc* retrovirus fail to form tumors in previous studies [8, 9]. To uncover the reasons for this, we examined cell fate of $Sox2^+$ cells infected with *MYC* lentivirus or $CD133^+$ cells infected with *Myc* retrovirus shortly after transplantation. Two days after transplantation, we found that all *MYC* lentivirus infected cells were $Sox2^+$, while only rare *Myc* retrovirus infected cells were $Sox2^+$ (Fig. 4F), suggesting that *Myc* retrovirus did not infect the $Sox2^+$ subpopulation in $CD133^+$ cells. Few $CC\text{-}3^+$ cells were detectable in either *MYC* virus infected $CD133^+$ cells or $Sox2^+$ cells at day 2 or day 9. At day 14, however, CC-3 staining was abundant in the transplanted $CD133^+$ cells whereas few $CC\text{-}3^+$ cells were observed in the transplanted $Sox2^+$ cells (Fig. 4F). $Sox2^+$ cells infected with *MYC* lentivirus further grew tumors while $CD133^+$ cells infected with *Myc* retrovirus did not, even though the *MYC* levels achieved by these viruses were similar (Supplementary Fig. S5B and C). These observations suggest that similar level of *MYC* induce different levels of apoptosis in $Sox2^+$ cells vs. $CD133^+$ cells, which may render these cells differentially susceptible to *MYC*-induced transformation.

Sox2 Promotes *MYC*-induced Tumorigenesis

The observation that *MYC*-driven tumors predominantly arise from $Sox2^+$ cells, without requiring other mutations, prompted the question whether *Sox2* itself plays a critical role in *MYC*-induced tumorigenesis. We first determined whether knockout of *Sox2* affected *MYC*-induced apoptosis in $Sox2^+$ cells. P5 Sox2-$CreER^{T2}/Sox2^{-loxp}$ mice were treated with tamoxifen to knockout *Sox2* in $Sox2^+$ cells and brain tissue was collected at P10. In the absence of tamoxifen treatment, Sox2 expression was co-localized with Sox9. With tamoxifen treatment, Sox2 was completely deleted, but Sox9 expression was not affected (Fig. 5A and B). Thus Sox9 traced the presence of $Sox2^+$ cells when *Sox2* is knocked out. Moreover, no CC-3 staining was observed in *Sox2* knockout cells (Fig. 5C and D). These data suggest that deletion of *Sox2* did not affect survival of $Sox2^+$ cells. We then examined CC-3 expression in $Sox2^+$ cells or *Sox2* knockout cells isolated from tamoxifen treated Sox2-$CreER^{T2}$/tdTomato or Sox2-$CreER^{T2}/Sox2^{-loxp}$/tdTomato mice and infected with control or *MYC* lentivirus *in vitro*. The result showed that *MYC* overexpression markedly

induced CC-3 expression in *Sox2* knockout cells but not in Sox2$^+$ cells (Fig. 5E), suggesting that *Sox2* antagonizes *MYC*-induced apoptosis.

Second, we tested whether *Sox2* deletion in Sox2$^+$ cells affected their susceptibility to *MYC*-induced transformation. Total cerebellar cells isolated from P5 mice of Sox2-CreER^{T2}/Sox2^{loxp} or Sox2-CreER^{T2} were infected with *MYC* lentivirus, cultured with or without 4-OHT for 16 hour and transplanted into the cerebella of NSG. 4-OHT treatment itself (i.e. in the absence of *Sox2* deletion) did not affect tumor growth, while deletion of *Sox2* was associated with significantly decreased tumor penetrance and increased tumor latency (Fig. 5F). Sox2 expression was not detected in the tumors generated from 4-OHT treated cells compared to control tumors (Supplementary Fig. S6A and B). *Sox2* knockout delayed tumor growth but did not completely prevent tumorigenesis. We reasoned that high levels of *Sox1*, *Sox3*, *Sox8* and *Sox10* expression in Sox2$^+$ cells (Supplementary Fig. S6C–F) may partially compensate for loss of *Sox2* function [30, 31].

Third, we determined whether overexpression of *Sox2* in Sox2$^-$ cells could promote *MYC*-induced tumorigenesis. Sox2$^-$ cells overexpressing *MYC* alone did not give rise to tumors, while mice receiving Sox2$^-$ cells overexpressing *MYC*/*Sox2* or *MYC*/*DNp53* and Sox2$^+$ cells overexpressing *MYC* developed tumors with LCA histology (Fig. 5G and H, Supplementary Fig. S6G). We further evaluated the role of *Sox2* in tumor initiation and progression. Sox2$^-$ cells were infected with viruses encoding *MYC* and Dox-inducible *Sox2* and transplanted into the cerebellum. Following transplantation, mice were fed Dox supplemented diet to induce *Sox2* expression for the first 10 days. Subsequently the mice were switched to a normal diet to eliminate *Sox2* expression. Eliminating *Sox2* expression did not affect tumor development (Fig. 5I), indicating that *Sox2* promotes the onset of *MYC*-induced tumorigenesis but is not required for tumor progression.

Sox2$^+$/Aldh1L1^{low} and Sox2$^+$/Aldh1L1^{neg} cells express *Sox2*, but they failed to develop *MYC*-driven tumors. *Sox2* levels in Sox2$^+$/Aldh1L1^{low} and Sox2$^+$/Aldh1L1^{neg} cells were significantly lower than in Sox2$^+$/Aldh1L1^{high} cells (Fig. 5J), which may account for the nonsusceptibility of Sox2$^+$/Aldh1L1^{low} and Sox2$^+$/Aldh1L1^{neg} cells to *MYC*-induced transformation.

Transcriptional Profiling Identifies Pathways Involved in the Growth of Murine *MYC*-Driven Medulloblastoma

To identify potential therapeutic targets for treating *MYC*-driven medulloblastoma, we compared the gene expression profiles of SOX2 tumors to those of freshly isolated Sox2$^+$ and Math1$^+$ postnatal cerebellar cells. PCA showed that the tumor cells were distinct from Sox2$^+$ cells from which they were derived and also distinct from Math1$^+$ GNPs (Fig. 6A). Hierarchical clustering confirmed that the SOX2 tumors differed from their normal cell counterpart (Fig. 6B). Focusing on 2-fold and higher changes in gene expression (p-value with FDR correction < 0.05), we identified 1013 upregulated and 896 downregulated genes in SOX2 tumors compared to Sox2$^+$ cerebellar cells (Supplementary Table S6).

To gain insight into the pathways controlling the growth of mouse *MYC*-driven tumors, we studied genes differentially expressed in tumors *vs.* normal cerebellar cells using functional

enrichment analysis (KEGG pathway annotation). The analysis showed that the genes upregulated in *MYC*-driven tumors were associated with ribosome biogenesis, RNA polymerase, RNA transport, metabolic pathways and glycolysis/gluconeogenesis (Fig. 6C and Supplementary Table S7).

Targeting LDHA Inhibits the Growth of *MYC*-driven Medulloblastoma

Upregulated expression of genes associated with glycolysis in mouse *MYC*-driven medulloblastoma suggested that the rapid proliferation of tumor cells may rely on this pathway, and that targeting this pathway may inhibit tumor growth. By RNA-Seq analysis, we found upregulation of genes encoding key enzymes controlling glucose metabolism including *Ldha*, *Pkm2* (Pyruvate kinase muscle isozyme M2), *Hk2* (Hexokinase 2) and *Pdk1* (Pyruvate Dehydrogenase Kinase 1) in SOX2 tumor cells compared to $Sox2^+$ normal cerebellar cells (Fig. 6D and Supplementary Table S8). qRT-PCR and western blot analysis confirmed the upregulation of these genes at mRNA and protein levels in SOX2 tumors compared to normal cerebellar cells or mouse SHH medulloblastoma (Fig. 6E and F). To determine whether growth of mouse *MYC*-driven tumors was dependent on glucose metabolism, we tested the effects of LDHA, PKM2 and PDK1 antagonists on tumor cell growth *in vitro*. GSK 2837808a and FX11, two antagonists of LDHA dramatically inhibited the growth of SOX2 tumor cells but exhibited minimal growth inhibition on mouse SHH tumor cells (Fig. 6G and H). In contrast, neither Pyruvate Kinase Inhibitor III (PKI-III, PKM2 antagonist) nor Dichloroacetate (DCA, PDK1 antagonist) showed inhibitory effects, even at the highest concentration (Fig. 6I and J). LDHA inhibitor had little effect on viability of normal cerebellar cells (GNPs) (Fig. 6K).

LDHA, *PKM2*, *HK2* and *PDK1* expression was also upregulated in human Group 3 medulloblastoma compared to normal cerebellar tissue or other subtypes of medulloblastoma (Fig. 7A and B, Supplementary Table S9). LDHA antagonists dramatically inhibited the growth of Group 3 PDX cells but showed minimal growth inhibition on SHH subgroup PDX cells (Fig. 7C and D). Neither PKM2 antagonist nor PDK1 antagonist showed inhibitory effects, even at the highest concentration (Fig. 7E and F). LDHA catalyzes the conversion of pyruvate to lactate [32]. We thus analyzed lactate production in Group 3 medulloblastoma PDX cells treated with LDHA antagonist. We found that inhibition of LDHA significantly decreased lactate levels in Group 3 PDX cells compared to control (Fig. 7G).

Further studies showed that *LDHA* expression was positively correlated with *MYC* (Fig. 7H, I and Supplementary Table S9) and associated with poor prognosis in human Group 3 medulloblastoma (Fig. 7J and Supplementary S7A). Knockdown of *LDHA* significantly reduced viability of Group 3 PDX cells *in vitro* (Fig. 7K, L, Supplementary S7B and C) and tumor growth *in vivo* (Fig. 7M), indicating that Group 3 medulloblastoma growth is dependent on *LDHA*. In contrast, knockdown of *LDHA* did not affect the viability of SHH PDX cells *in vitro* (Supplementary Fig. S7D). In addition, *LDHA* knockdown did not affect *MYC* expression in Group 3 PDX cells (Supplementary Fig. S7E).

Discussion

The present work demonstrates that *MYC* overexpression alone, in the absence of other genetic alterations, can drive tumorigenesis from astrocyte progenitors in the postnatal cerebellum. The tumors accurately model human Group 3 medulloblastoma associated with amplification of *MYC* and therefore provide a valuable tool for the evaluation of novel therapies. By studying this novel mouse model, we identified *LDHA* as a specific target for the development of less toxic therapies for this highly malignant disease.

Sox2$^+$ astrocyte progenitors are susceptible to *MYC* transformation

MYC-induced tumorigenesis often requires a defined range of *MYC* levels. Excessive activation of *MYC* is associated with DNA damage and apoptosis, while less robust *MYC* activation induces proliferative arrest and cellular senescence [33, 34]. In previously described Group 3 medulloblastoma mouse models, *in utero* electroporation of *MYC* plasmid into distinct populations of embryonic cerebellar progenitor cells did not induce tumors [10], possibly because *MYC* levels achieved by this approach were too low to overcome proliferation arrest. In other models [8, 9], inactivation of *Trp53* was required for *MYC*-induced tumorigenesis, suggesting that inactivation of *Trp53* may be required to overcome the *MYC*-induced apoptosis in those cells.

MYC-induced transformation also depends on genetic and epigenetic cellular context [15, 35]. *Mycn* overexpression failed to initiate tumor formation in several experimental models [36, 37] but was shown to transform Glt1-positive glial cells and certain distinct neural stem cell populations [38, 39], suggesting that distinct cell types are susceptible to *Mycn*-induced tumorigenesis. Our studies show that Sox2$^+$ astrocyte progenitors in the postnatal cerebellum are susceptible to *MYC*-induced tumorigenesis and *Sox2* itself plays a critical role in this process. *Sox2* has been reported to play important roles in cancer, where it promotes tumor cell proliferation, colony formation and self-renewal of cancer stem cells (CSCs) [40, 41]. Here, we report that *Sox2* is critical for *MYC*-induced tumor initiation. We demonstrated that *Sox2* antagonized *MYC*-induced apoptosis in Sox2$^+$ cerebellar cells and knockout of *Sox2* in these cells significantly delayed the formation of *MYC*-driven tumors. Moreover, overexpression of *Sox2* promoted *MYC*-induced tumorigenesis from Sox2$^-$ cells, which otherwise cannot be transformed by *MYC* overexpression alone. In this process, *Sox2* was only required for tumor initiation, but not for tumor progression. A subpopulation of CD133$^+$ cells expressed *Sox2* (CD133$^+$/Sox2$^+$), but CD133$^+$ cells infected with *Myc* retrovirus failed to form tumors. The observation that the Sox2$^+$ subpopulation in CD133$^+$ cells was not infected by *Myc* retrovirus and that *Myc* retrovirus infected cells underwent dramatic apoptosis post-transplantation may explain the failure of these cells to form tumors. Sox2$^+$/Aldh1L1^{low} and Sox2$^+$/Aldh1L1^{neg} cells also expressed *Sox2*, but they were not susceptible to *MYC*-induced transformation. These cells had very limited capacity for self-renewal and expressed significantly lower levels of *Sox2* compared to Sox2$^+$/Aldh1L1^{high} cells. *Sox2* expression levels are linked to maintenance of progenitor cell identity and increased capacity for self-renewal [42]. We therefore reasoned that the differential tumorigenesis potential of distinct Sox2$^+$ subpopulations may be related to *Sox2* levels.

SOX2 tumors included quiescent $Sox2^+$ cells comprising less than 5% of the tumor cell population. Rare and quiescent $Sox2^+$ cells have also been observed in SHH subgroup medulloblastoma, where they were identified as CSCs driving tumor progression and contributing to treatment resistance [43]. It will be of great interest to determine in future studies whether $Sox2^+$ cells in *MYC*-driven medulloblastoma are also CSCs and whether these cells contribute to treatment resistance and therapeutic failure.

Identification of *LDHA* as a novel therapeutic target for *MYC*-driven medulloblastoma

In order to identify novel therapeutic targets for *MYC*-driven medulloblastoma treatment, we compared the gene expression profiles of mouse *MYC*-driven tumors to those of normal cerebellar cells from which they were derived. In addition to the identification of pathways that are reportedly enriched in human Group 3 medulloblastoma such as ribosome biogenesis, RNA polymerase, and RNA transport [5], our gene expression analysis also revealed upregulation of genes involved in glycolysis, which has not been previously well studied in *MYC*-driven medulloblastoma.

Cancer cells predominantly produce energy through a high rate of glycolysis with secretion of lactate even under conditions of abundant oxygen [44], a process called aerobic glycolysis or the Warburg effect. The key enzymes involved in aerobic glycolysis, including HK2, PKM2, PDK1 and LDHA, have been identified as potential targets for therapeutic intervention in many cancers, including pediatric brain tumors. Deletion of the gene encoding HK2 in the developing brain was shown to inhibit SHH-induced aerobic glycolysis and reduce SHH-associated medulloblastoma growth [45], while *PKM2* deletion accelerated the growth of SHH-associated medulloblastoma [46]. The roles of *PDK1* and *LDHA* in medulloblastoma have not previously been evaluated.

In the current study, we found that PKM2 and PDK1 inhibition did not affect growth of *MYC*-driven tumors. In contrast, inhibition of LDHA significantly reduced growth of *MYC*-driven medulloblastoma with reduced secretion of lactate, but had minimal effects on growth of SHH-associated medulloblastoma or normal cerebellar cells. The *LDHA* gene is known to be regulated by *MYC* [47, 48] and *HIF1A* [49]. However, we did not observe upregulation of *HIF1A* in either mouse or human *MYC*-driven medulloblastoma. We therefore suggested that upregulation of *LDHA* is very likely a result of *MYC* overexpression in Group 3 medulloblastoma. This is supported by our observation that *LDHA* expression was positively correlated with *MYC* levels and associated with poor prognosis.

Our studies present the first evidence that targeting *LDHA* effectively inhibits growth of *MYC*-driven medulloblastoma, but not *MYC*-independent tumors or normal cerebellar cells. While the results presented here are promising, existing LDHA inhibitors are not amenable to immediate preclinical translational studies due to low blood-brain barrier penetrance [50]. Nevertheless, our findings warrant further studies and should act as a spur to efforts to develop LDHA antagonists clinically suitable for the treatment of *MYC*-driven medulloblastoma patients.

Supplementary Material

Refer to Web version on PubMed Central for supplementary material.

Acknowledgements

The authors would like to acknowledge Jeffery Rothstein for Aldh1L1^{-GFP} mice and Baljit Khakh for Aldh1L1-CreER^{T2} mice; Daniel Treisman, Yuan Zhu and Zeng-jie Yang for providing mouse SHH medulloblastoma cells or cell pellets; Mirna Lechpammer for normal childhood cerebellar tissue; Huadong Pei for LDHA shRNA, William Hahn for GFP shRNA, Scott Lowe for MSCV-IRES-Luciferase and Didier Trono for pWPI plasmids; Yoon-Jae Cho, Robert Wechsler-Reya, Xiao-Nan Li and James Olson for the PDX lines; Robert Wechsler-Reya for helpful discussions and Adam Richman and Naomi Luban for editing the manuscript. This work was supported by funds from Children's National Health Systems, NIH R21CA180063 (YPEI) and R21NS102776 (YPEI).

References

1. Packer RJ, et al., Medulloblastoma and primitive neuroectodermal tumors. Handb Clin Neurol, 2012 105: p. 529–48. [PubMed: 22230517]
2. Northcott PA, et al., The whole-genome landscape of medulloblastoma subtypes. Nature, 2017 547(7663): p. 311–317. [PubMed: 28726821]
3. Cho YJ, et al., Integrative genomic analysis of medulloblastoma identifies a molecular subgroup that drives poor clinical outcome. J Clin Oncol, 2011 29(11): p. 1424–30. [PubMed: 21098324]
4. Kool M, et al., Molecular subgroups of medulloblastoma: an international meta-analysis of transcriptome, genetic aberrations, and clinical data of WNT, SHH, Group 3, and Group 4 medulloblastomas. Acta Neuropathol, 2012 123(4): p. 473–84. [PubMed: 22358457]
5. Cavalli FMG, et al., Intertumoral Heterogeneity within Medulloblastoma Subgroups. Cancer Cell, 2017 31(6): p. 737–754 e6. [PubMed: 28609654]
6. Taylor MD, et al., Molecular subgroups of medulloblastoma: the current consensus. Acta Neuropathol, 2012 123(4): p. 465–72. [PubMed: 22134537]
7. Northcott PA, et al., Enhancer hijacking activates GFI1 family oncogenes in medulloblastoma. Nature, 2014 511(7510): p. 428–34. [PubMed: 25043047]
8. Pei Y, et al., An animal model of MYC-driven medulloblastoma. Cancer Cell, 2012 21(2): p. 155–67. [PubMed: 22340590]
9. Kawauchi D, et al., A mouse model of the most aggressive subgroup of human medulloblastoma. Cancer Cell, 2012 21(2): p. 168–80. [PubMed: 22340591]
10. Kawauchi D, et al., Novel MYC-driven medulloblastoma models from multiple embryonic cerebellar cells. Oncogene, 2017 36(37): p. 5231–5242. [PubMed: 28504719]
11. Hill RM, et al., Combined MYC and P53 defects emerge at medulloblastoma relapse and define rapidly progressive, therapeutically targetable disease. Cancer Cell, 2015 27(1): p. 72–84. [PubMed: 25533335]
12. Zhukova N, et al., Subgroup-specific prognostic implications of TP53 mutation in medulloblastoma. J Clin Oncol, 2013 31(23): p. 2927–35. [PubMed: 23835706]
13. Pelengaris S, Rudolph B, and Littlewood T, Action of Myc in vivo - proliferation and apoptosis. Curr Opin Genet Dev, 2000 10(1): p. 100–5. [PubMed: 10679391]
14. Murphy DJ, et al., Distinct Thresholds Govern Myc's Biological Output In Vivo. Cancer Cell, 2008 14(6): p. 447–57. [PubMed: 19061836]
15. Beer S, et al., Developmental context determines latency of MYC-induced tumorigenesis. PLoS Biol, 2004 2(11): p. e332. [PubMed: 15455033]
16. Gabay M, Li Y, and Felsher DW, MYC activation is a hallmark of cancer initiation and maintenance. Cold Spring Harb Perspect Med, 2014 4(6).
17. Baudino TA, et al., Myc-mediated proliferation and lymphomagenesis, but not apoptosis, are compromised by E2f1 loss. Mol Cell, 2003 11(4): p. 905–14. [PubMed: 12718877]
18. Gibson P, et al., Subtypes of medulloblastoma have distinct developmental origins. Nature, 2010 468(7327): p. 1095–9. [PubMed: 21150899]

19. Yang ZJ, et al., Medulloblastoma can be initiated by deletion of Patched in lineage-restricted progenitors or stem cells. Cancer Cell, 2008 14(2): p. 135–45. [PubMed: 18691548]
20. Schuller U, et al., Acquisition of granule neuron precursor identity is a critical determinant of progenitor cell competence to form Shh-induced medulloblastoma. Cancer Cell, 2008 14(2): p. 123–34. [PubMed: 18691547]
21. Bandopadhayay P, et al., BET bromodomain inhibition of MYC-amplified medulloblastoma. Clin Cancer Res, 2014 20(4): p. 912–25. [PubMed: 24297863]
22. Zhao X, et al., Global gene expression profiling confirms the molecular fidelity of primary tumor-based orthotopic xenograft mouse models of medulloblastoma. Neuro Oncol, 2012 14(5): p. 574–83. [PubMed: 22459127]
23. Girard E, et al., Efficacy of cabazitaxel in mouse models of pediatric brain tumors. Neuro Oncol, 2015 17(1): p. 107–15. [PubMed: 25140037]
24. Morfouace M, et al., Pemetrexed and gemcitabine as combination therapy for the treatment of Group3 medulloblastoma. Cancer Cell, 2014 25(4): p. 516–29. [PubMed: 24684846]
25. Brun SN, et al., Survivin as a therapeutic target in Sonic hedgehog-driven medulloblastoma. Oncogene, 2015 34(29): p. 3770–9. [PubMed: 25241898]
26. Arnold K, et al., Sox2(+) adult stem and progenitor cells are important for tissue regeneration and survival of mice. Cell Stem Cell, 2011 9(4): p. 317–29. [PubMed: 21982232]
27. Madisen L, et al., A robust and high-throughput Cre reporting and characterization system for the whole mouse brain. Nat Neurosci, 2010 13(1): p. 133–40. [PubMed: 20023653]
28. Yang Y, et al., Molecular comparison of GLT1+ and ALDH1L1+ astrocytes in vivo in astroglial reporter mice. Glia, 2011 59(2): p. 200–7. [PubMed: 21046559]
29. Lee A, et al., Isolation of neural stem cells from the postnatal cerebellum. Nat Neurosci, 2005 8(6): p. 723–9. [PubMed: 15908947]
30. Graham V, et al., SOX2 functions to maintain neural progenitor identity. Neuron, 2003 39(5): p. 749–65. [PubMed: 12948443]
31. Collignon J, et al., A comparison of the properties of Sox-3 with Sry and two related genes, Sox-1 and Sox-2. Development, 1996 122(2): p. 509–20. [PubMed: 8625802]
32. Le A, et al., Inhibition of lactate dehydrogenase A induces oxidative stress and inhibits tumor progression. Proc Natl Acad Sci U S A, 2010 107(5): p. 2037–42. [PubMed: 20133848]
33. Felsher DW, et al., Overexpression of MYC causes p53-dependent G2 arrest of normal fibroblasts. Proc Natl Acad Sci U S A, 2000 97(19): p. 10544–8. [PubMed: 10962037]
34. Grandori C, et al., Werner syndrome protein limits MYC-induced cellular senescence. Genes Dev, 2003 17(13): p. 1569–74. [PubMed: 12842909]
35. Li Y, Casey SC, and Felsher DW, Inactivation of MYC reverses tumorigenesis. J Intern Med, 2014 276(1): p. 52–60. [PubMed: 24645771]
36. Browd SR, et al., N-myc can substitute for insulin-like growth factor signaling in a mouse model of sonic hedgehog-induced medulloblastoma. Cancer Res, 2006 66(5): p. 2666–72. [PubMed: 16510586]
37. McCall TD, Pedone CA, and Fults DW, Apoptosis suppression by somatic cell transfer of Bcl-2 promotes Sonic hedgehog-dependent medulloblastoma formation in mice. Cancer Res, 2007 67(11): p. 5179–85. [PubMed: 17545597]
38. Swartling FJ, et al., Pleiotropic role for MYCN in medulloblastoma. Genes Dev, 2010 24(10): p. 1059–72. [PubMed: 20478998]
39. Swartling FJ, et al., Distinct neural stem cell populations give rise to disparate brain tumors in response to N-MYC. Cancer Cell, 2012 21(5): p. 601–13. [PubMed: 22624711]
40. Chou YT, et al., The emerging role of SOX2 in cell proliferation and survival and its crosstalk with oncogenic signaling in lung cancer. Stem Cells, 2013 31(12): p. 2607–19. [PubMed: 23940081]
41. Boumahdi S, et al., SOX2 controls tumour initiation and cancer stem-cell functions in squamous-cell carcinoma. Nature, 2014 511(7508): p. 246–50. [PubMed: 24909994]
42. Hutton SR and Pevny LH, SOX2 expression levels distinguish between neural progenitor populations of the developing dorsal telencephalon. Dev Biol, 2011 352(1): p. 40–7. [PubMed: 21256837]

43. Vanner RJ, et al., Quiescent sox2(+) cells drive hierarchical growth and relapse in sonic hedgehog subgroup medulloblastoma. Cancer Cell, 2014 26(1): p. 33–47. [PubMed: 24954133]
44. Liberti MV and Locasale JW, The Warburg Effect: How Does it Benefit Cancer Cells? Trends Biochem Sci, 2016 41(3): p. 211–218. [PubMed: 26778478]
45. Gershon TR, et al., Hexokinase-2-mediated aerobic glycolysis is integral to cerebellar neurogenesis and pathogenesis of medulloblastoma. Cancer Metab, 2013 1(1): p. 2. [PubMed: 24280485]
46. Tech K, et al., Pyruvate Kinase Inhibits Proliferation during Postnatal Cerebellar Neurogenesis and Suppresses Medulloblastoma Formation. Cancer Res, 2017 77(12): p. 3217–3230. [PubMed: 28515149]
47. Lewis BC, et al., Identification of putative c-Myc-responsive genes: characterization of rcl, a novel growth-related gene. Mol Cell Biol, 1997 17(9): p. 4967–78. [PubMed: 9271375]
48. Shim H, et al., *c*-Myc transactivation of LDH-A: implications for tumor metabolism and growth. Proc Natl Acad Sci U S A, 1997 94(13): p. 6658–63. [PubMed: 9192621]
49. Semenza GL, et al., Hypoxia response elements in the aldolase A, enolase 1, and lactate dehydrogenase A gene promoters contain essential binding sites for hypoxia-inducible factor 1. J Biol Chem, 1996 271(51): p. 32529–37. [PubMed: 8955077]
50. Valvona CJ, et al., The Regulation and Function of Lactate Dehydrogenase A: Therapeutic Potential in Brain Tumor. Brain Pathol, 2016 26(1): p. 3–17. [PubMed: 26269128]

Significance:

Insights from a new model identified *LDHA* as a novel target for Group 3 medulloblastoma, paving the way for the development of effective therapies against this disease.

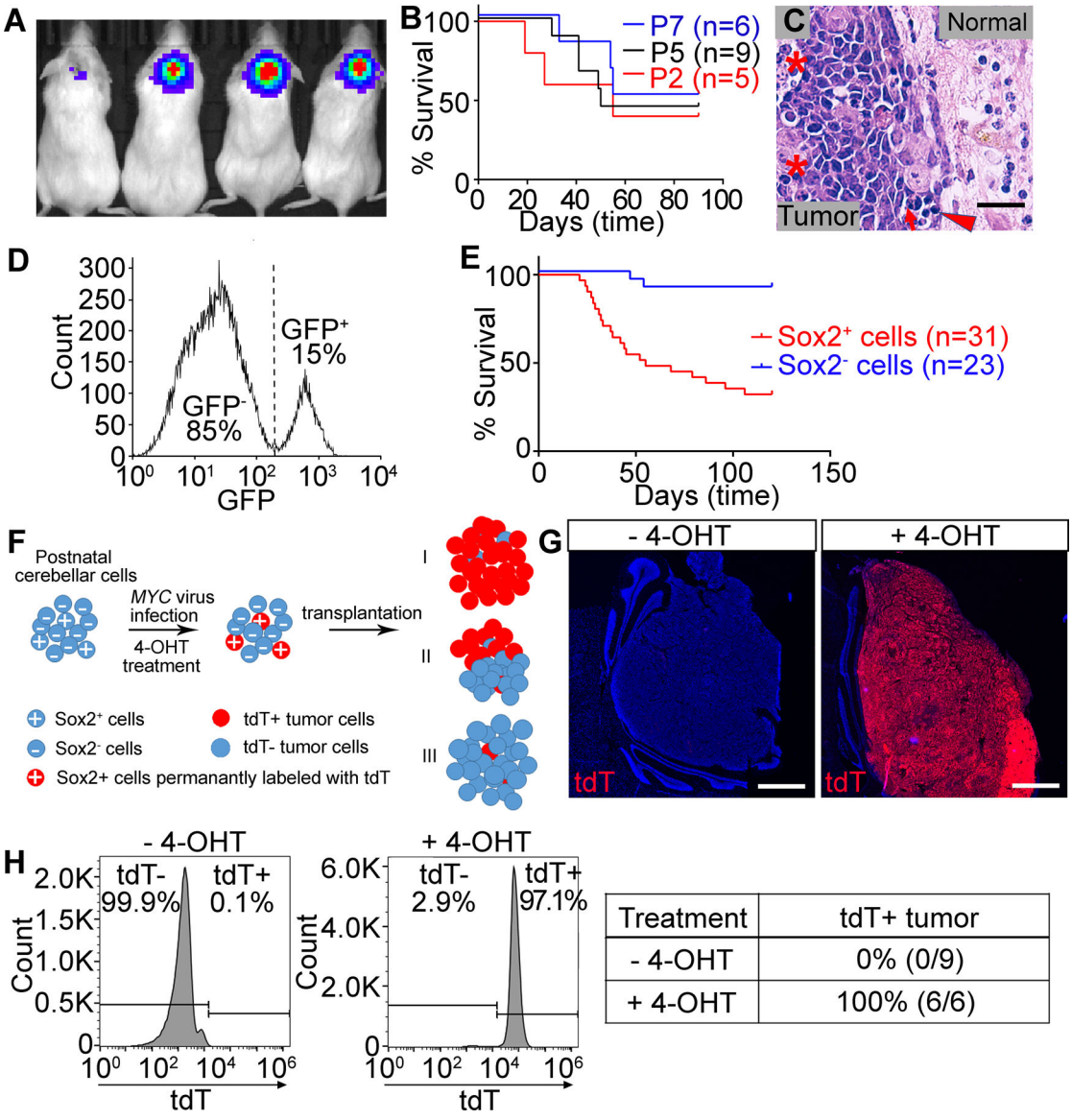

Treatment	tdT+ tumor
- 4-OHT	0% (0/9)
+ 4-OHT	100% (6/6)

Figure 1. *MYC* overexpression alone drives tumorigenesis from Sox2$^+$ cells in the postnatal cerebellum.

(A–C) Tumors generated from total cerebellar cells. (A) Bioluminescent imaging. (B) Survival curve. (C) H&E staining of tumor sections. Asterisks show an area of necrosis and a large tumor cell with marked nuclear atypia (anaplasia). Arrow shows prominent nuclear molding. Arrowhead shows mitotic figures. Normal indicates normal tissue. Scale bars = 25 μm. (D) FACS-sorting of Sox2$^+$ cells. (E) Survival curve of tumors generated from Sox2$^+$ or Sox2$^-$ cells. (F) Schema for identifying tumor cells-of-origin. (G) tdT expression in tumors generated from Sox2-CreER^{T2}/Rosa-CAG-LSL-tdTomato cells treated with or without 4-OHT. Nuclei were counter-stained with DAPI (blue). Scale bars = 1 mm. (H) Flow cytometry analysis of tdT expression in tumors from (G) and summary of percentage of tdT$^+$ tumors.

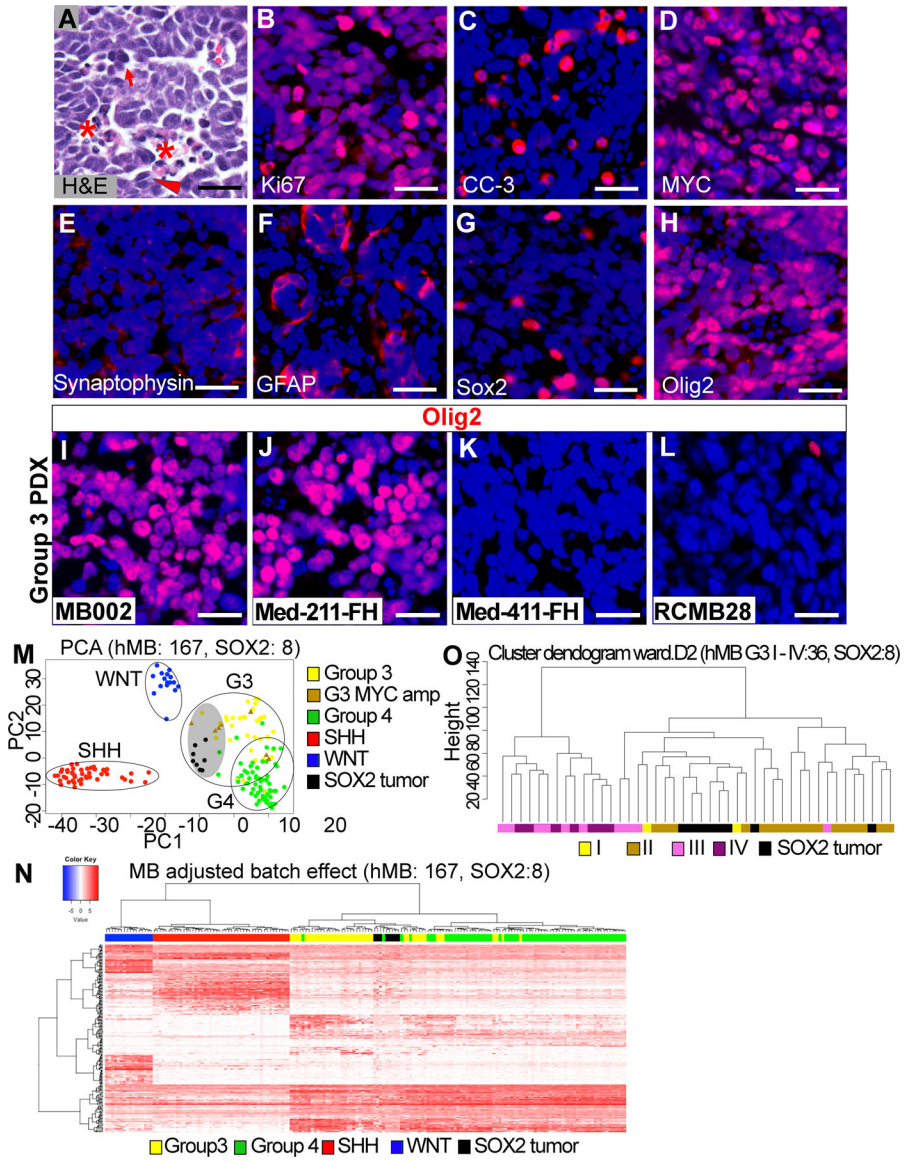

Figure 2. SOX2 tumors resemble Group 3 medulloblastoma at the cellular and molecular levels.

(A) H&E staining of tumor sections. Asterisks show an area of necrosis, and a large tumor cell with marked nuclear atypia (anaplasia). Arrow shows prominent nuclear molding. Arrowhead shows mitotic figures. (B–H) IHC staining of SOX2 tumor tissue. (I–L) Olig2 expression in human Group 3 medulloblastoma PDX. In all IHC staining, scale bars = 25 μm. (M) PCA for batch effect adjusted gene expression (RPKM) quantifies data from human medulloblastoma and SOX2 tumors for the top 500 most variable genes across the data set. (N) Unsupervised hierarchical clustering for four groups of human medulloblastoma and SOX2 tumor applied on ortholog subset from significant medulloblastoma group-specific differentially expressed genes. (O) Unsupervised hierarchical clustering of batch effect adjusted SOX2 tumors and Group3 medulloblastoma samples assigned with subtypes I, II, III and IV.

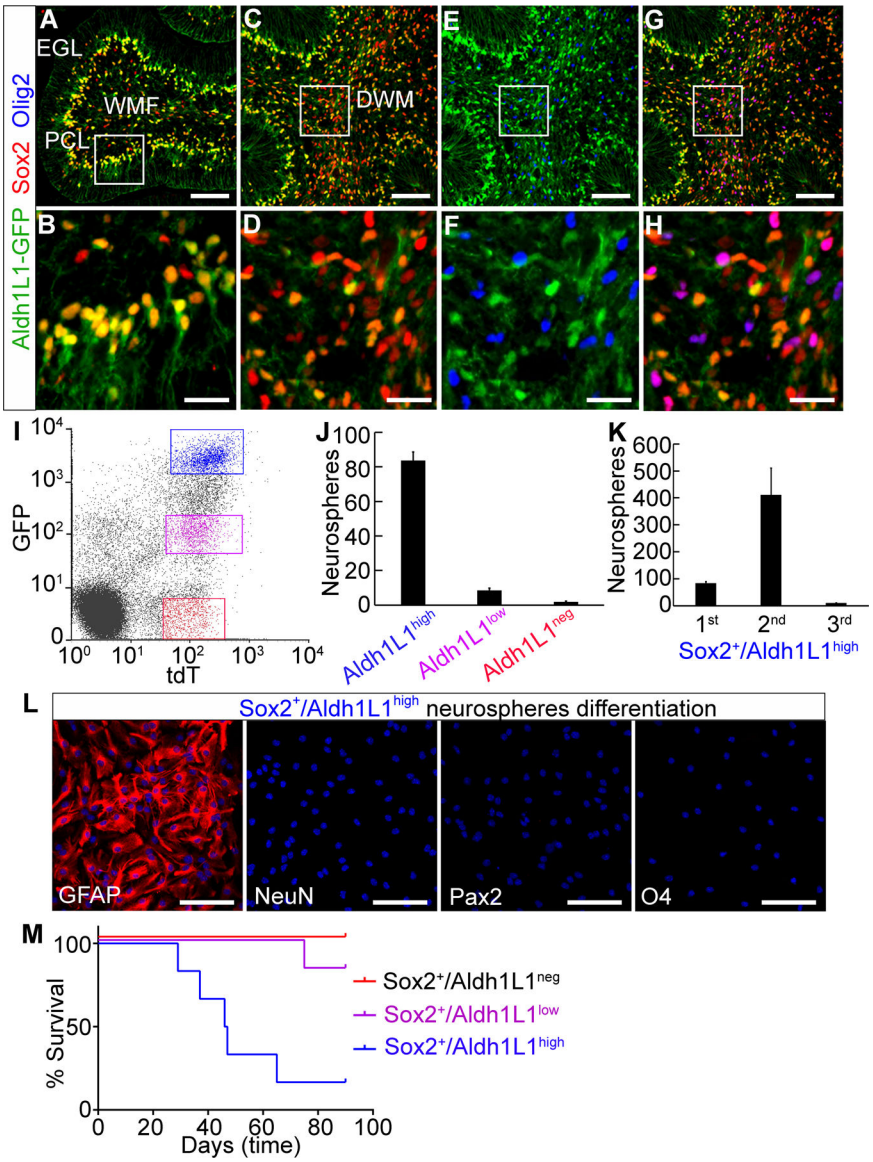

Figure 3. *MYC*-driven tumors arise from astrocyte progenitors.

(A–H) $Sox2^+$ cells are composed of $Aldh1L1^{high}$, $Aldh1L1^{low}$ and $Aldh1L1^{neg}$ cells. Scale bars = 100 μm. (B, D, F and H) High magnification images corresponding to the inset boxes in (A, C, E and G). Scale bars = 25 μm. (I) Isolation of $Sox2^+/Aldh1L1^{high}$, $Sox2^+/Aldh1L1^{low}$ and $Sox2^+/Aldh1L1^{neg}$ cells by flow cytometry. (J) Number of primary neurospheres from 5000 cells. (K) Number of primary, secondary or tertiary neurospheres from 5000 $Sox2^+/Aldh1L1^{high}$ cells. Error bars indicate mean ± SD. (L) Differentiation of primary neurospheres from $Sox2^+/Aldh1L1^{high}$ cells. Nuclei were counter-stained with DAPI (blue). Scale bars = 100 μm. (M) Survival curve (n=6 each).

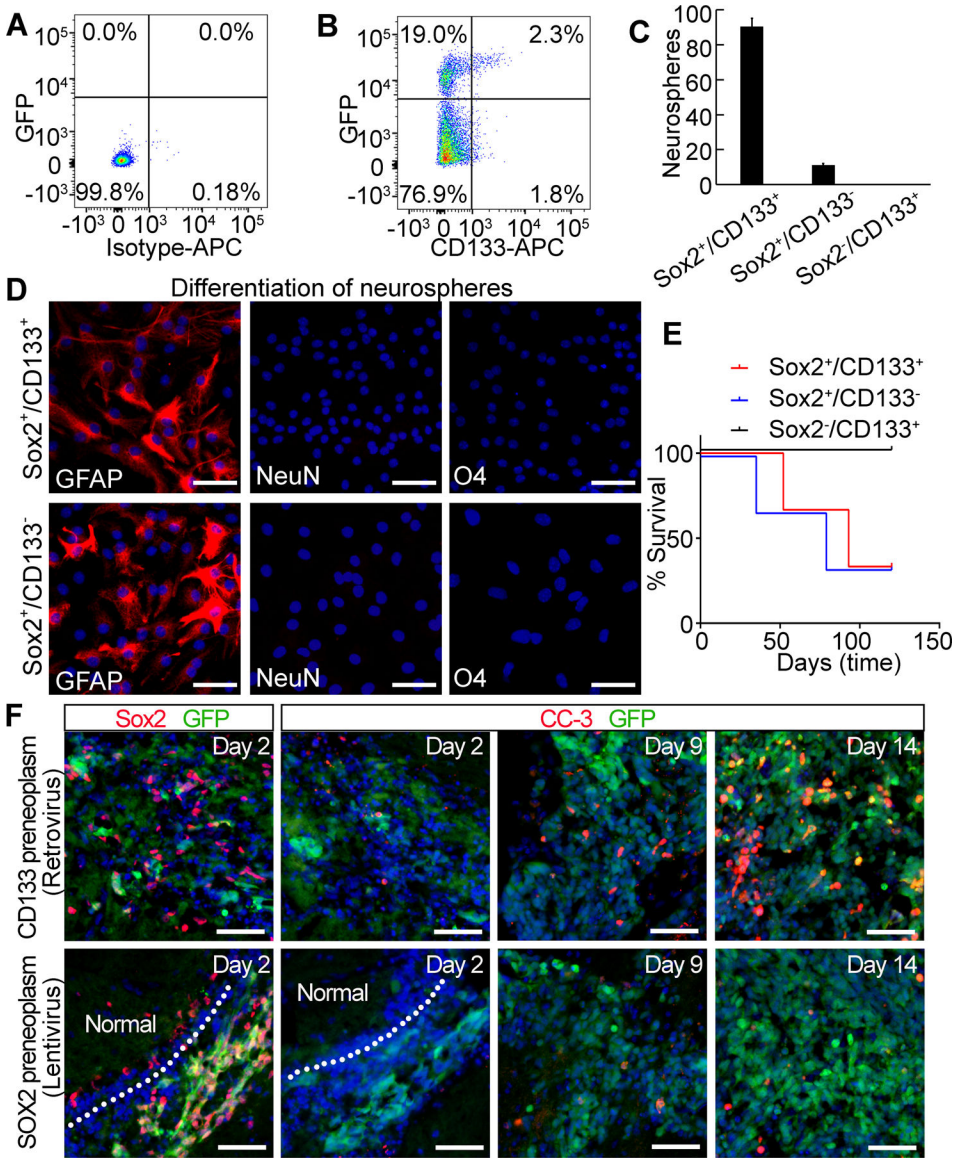

Figure 4. Characterization of Sox2^{+} vs. CD133^{+} cells in the early postnatal cerebellum.

(A) and (B) Expression of CD133 and Sox2 in the early postnatal cerebellum. Total cerebellar cells from P5 wild type (A) or Sox2^{-GFP} mice (B) were stained with APC conjugated isotype or anti-CD133 antibody and then analyzed for GFP or CD133 expression by flow cytometry. (C) Number of primary neurospheres from 5000 cells. (D) Differentiation of primary neurospheres. (E) Survival curve. (F) IHC staining for Sox2 or CC-3 in preneoplasms. GFP indicates *MYC* virus infected cells shown as green. Normal indicates normal tissue. In all IHC staining, scale bars = 50 μm and nuclei were counter-stained with DAPI (blue).

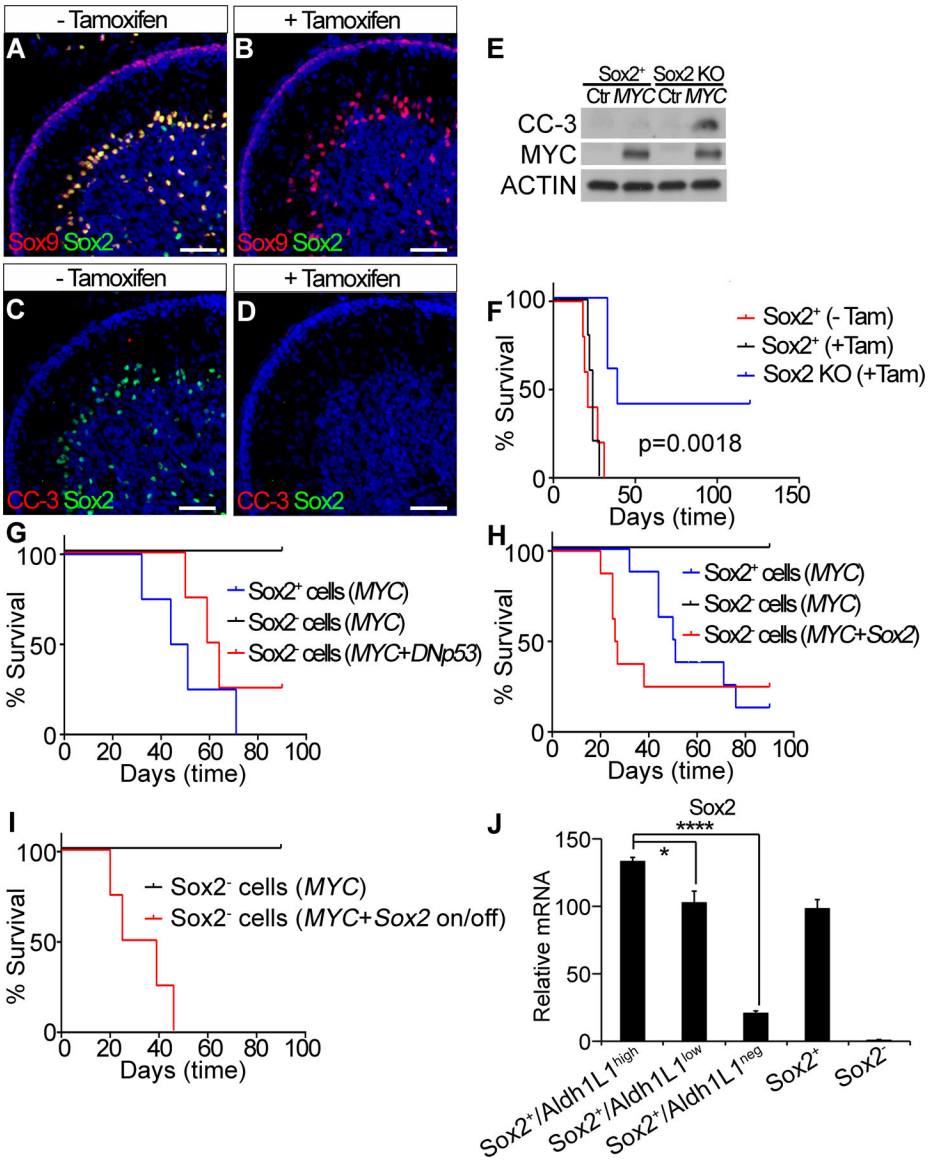

Figure 5. *Sox2* promotes *MYC*-induced tumorigenesis.

(A–D) IHC staining for Sox2, Sox9 or CC-3 in P10 cerebellum. Scale bars = 50 μm. Nuclei were counter-stained with DAPI (blue). (E) Expression of CC-3 assessed by western blot. (F) Survival curve of mice transplanted with cells from Sox2-CreER^{T2}/Sox2^{loxp} mice or Sox2-CreER^{T2} mice treated with or without tamoxifen (n=5 each). (G) Survival curve of mice transplanted with Sox2^{+} cells infected with *MYC* lentivirus or Sox2^{-} cells infected with viruses of *MYC* or *MYC* + *DNp53* (n=4 each). (H) Survival curve of mice transplanted with Sox2^{+} cells infected with *MYC* lentivirus or Sox2^{-} cells infected with viruses of *MYC* or *MYC* + *Sox2* (n=8 each). (I) Survival curve of mice transplanted with Sox2^{-} cells infected with viruses of *MYC* or *MYC* + *Sox2* (n=4 each). Exogenous Sox2 expression was shut off at 10 days after transplantation. (J) *Sox2* expression assessed by qRT-PCR. mRNA level in Sox2^{-} cells was set up to 1. Error bars indicate mean ± SD. *p<0.05, ****p<0.0001.

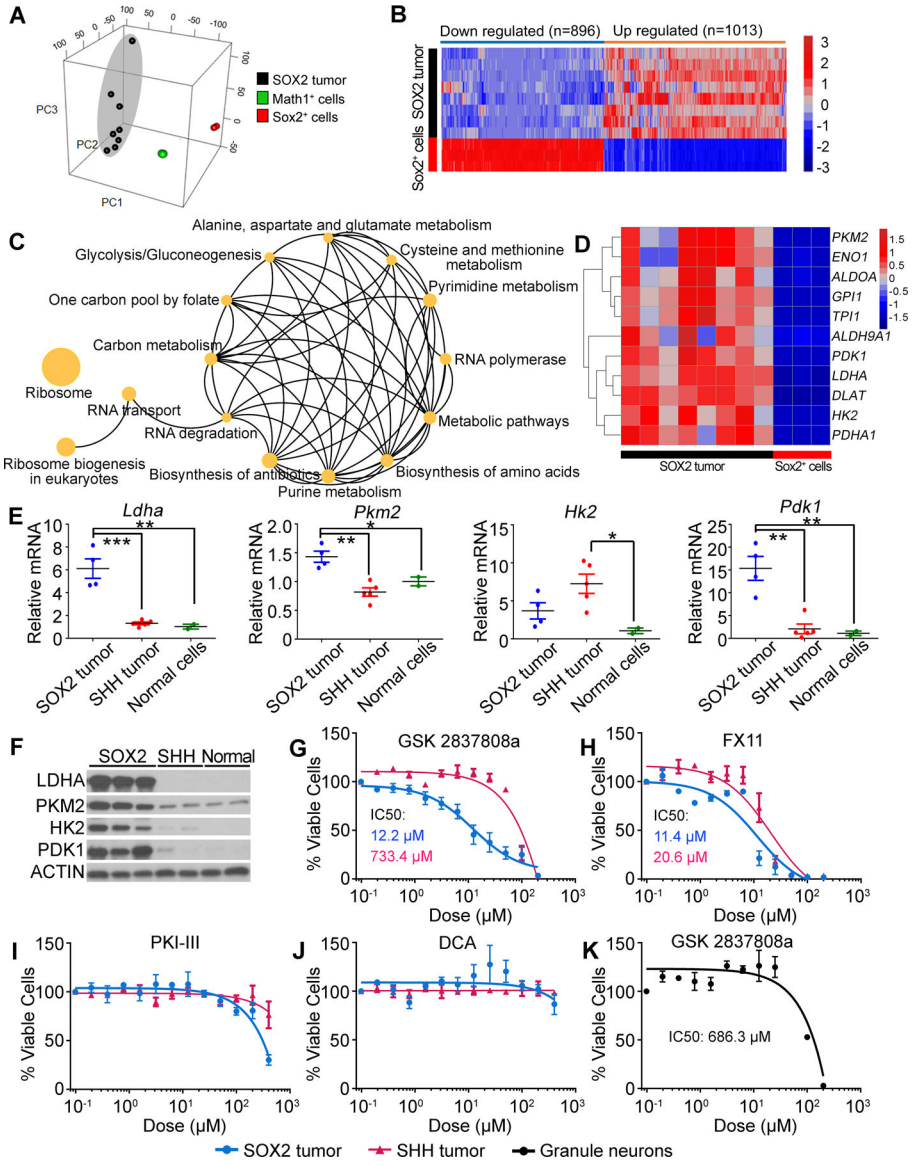

Figure 6. Inhibition of LDHA suppresses growth of mouse *MYC*-driven medulloblastoma.

(A) PCA of SOX2 tumors and P5 $Sox2^+$ and $Math1^+$ normal cerebellar cells using all genes exhibiting variation across the data set. (B) Heatmap showing dysregulated genes in SOX2 tumors compared with normal $Sox2^+$ cells. (C) Biological pathways enriched in SOX2 tumors. (D) Heatmap showing genes involved in glycolysis in SOX2 tumor and normal $Sox2^+$ cells. (E) Expression of *Ldha*, *Pkm2*, *Hk2* and *Pdk1* assessed by qRT-PCR. Mean mRNA value in normal cerebellar cells was set to 1. *p<0.05, **p<0.01, ***p<0.001. (F) Expression of *Ldha*, *Pkm2*, *Hk2* and *Pdk1* assessed by western blot. (G-J) Effect of LDHA inhibitors (G and H), PKM2 inhibitor (I) or PDK1 inhibitor (J) on growth of tumor cells *in vitro*. (K) Effect of LDHA inhibitor on viability of GNPs *in vitro*. Error bars indicate mean ± SEM.

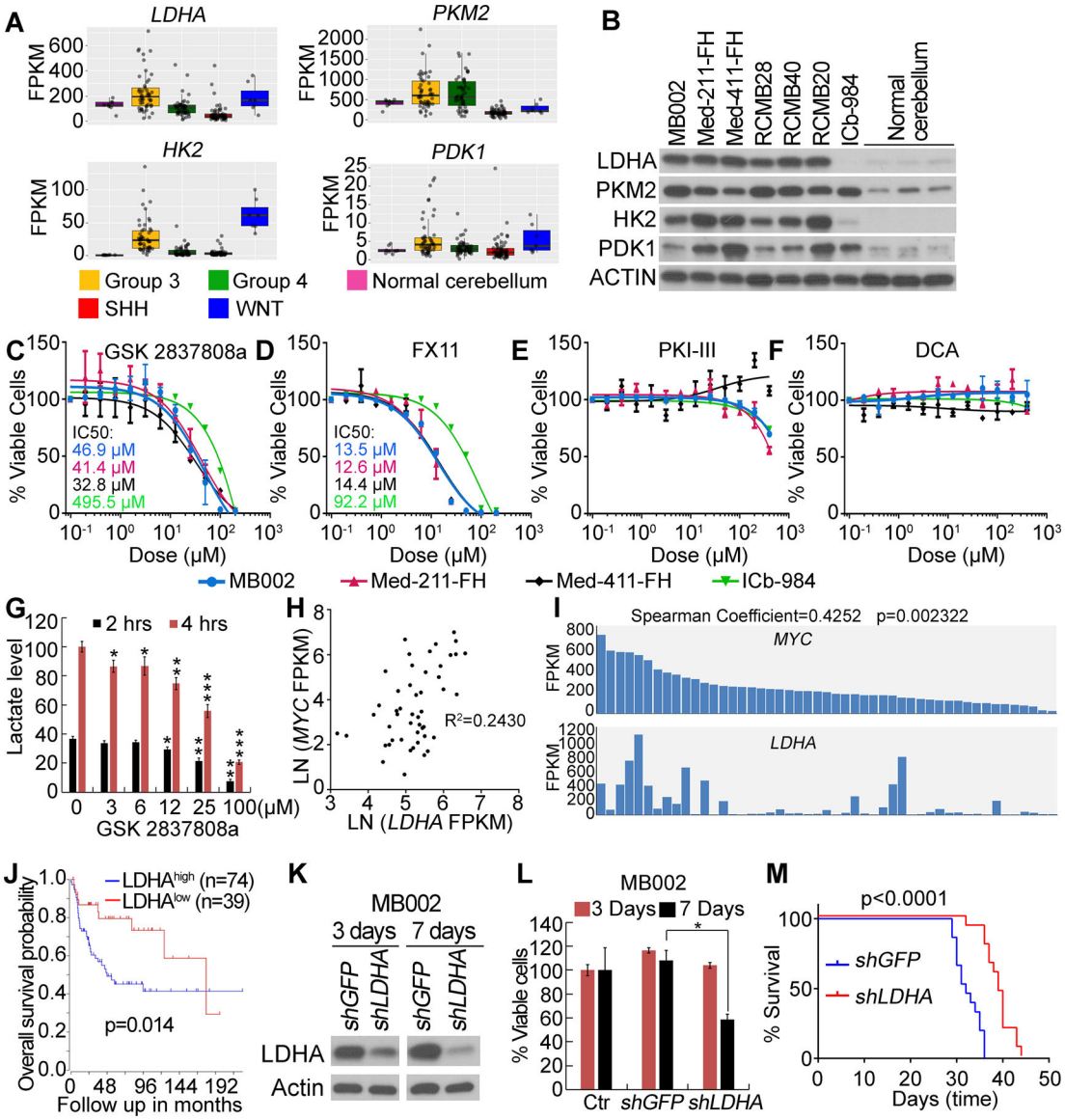

Figure 7. Inhibition of LDHA suppresses growth of human *MYC*-driven medulloblastoma.

(A) Expression of *LDHA*, *PKM2*, *HK2* and *PDK1* assessed by RNA-Seq. (B) Expression of *LDHA*, *PKM2*, *HK2* and *PDK1* in Group 3 and SHH Group medulloblastoma PDX or normal human cerebellum examined by western blot. (C–F) Effect of LDHA inhibitors (C and D), PKM2 inhibitor (E) or PDK1 inhibitor (F) on growth of PDX cells *in vitro*. Error bars in A, C–F indicate mean ± SEM. (G) Lactate levels in Group 3 PDX cells treated with LDHA inhibitor *in vitro*. Value of untreated sample collected at 4 hours was set to 100. (H) and (I) Positive correlation of *LDHA* and *MYC* expression in human Group 3 medulloblastoma. (H) Linear regression of *LDHA* and *MYC* mRNA level, R-squared is indicated. (I) Bar plot of *LDHA* and *MYC* mRNA levels. (J) Kaplan-Meier analysis of Group3 medulloblastoma patients. (K) Knockdown of *LDHA* in Group 3 PDX cells examined by western blot. (L) Knockdown of *LDHA* inhibits growth of Group 3 PDX cells *in vitro*. Viability of cells without virus infection (Ctr) was set to 100%. (M) Knockdown of

LDHA inhibits tumor growth of Group 3 PDX *in vivo*. n=10 in each group. In (G) and (L), error bars indicate mean ± SD. Asterisk represents statistical significance between indicated treated groups and untreated groups. *p<0.05, **p<0.01, ***p<0.001.